RADIO SCIENCE, VOL. 42, RS5003, doi:10.1029/2006RS003522, 2007



# Wavelet-like efficient analysis of two-dimensional arbitrarily shaped radomes using a surface formulation

F. D. Quesada-Pereira,[1] A. Vidal,[2] V. E. Boria,[2] A. Alvarez-Melcón,[1] and B. Gimeno[3]

Received 6 May 2006; revised 2 May 2007; accepted 12 July 2007; published 18 September 2007.

[1] Radomes are usually made of lossy dielectric materials, and their accurate analysis is often cumbersome because of their typical large electrical size and geometrical complexity. In real reflector antenna structures, there are always complex interactions between the radome, the reflector surfaces and the directional feeds, which are typically neglected for the sake of simplicity. In this paper we will consider all such interactions in a very accurate way, thus requiring a high number of unknowns for the numerical solution of the problem. To overcome such drawback, an integral equation formulation based on the Equivalence Principle in combination with the wavelet transform has been employed, obtaining finally a robust and accurate CAD tool for the rigorous analysis of arbitrarily shaped radomes containing continuous and discrete electromagnetic sources. It will be shown that the use of wavelet-like bases substantially improves the numerical efficiency and memory requirements of the original integral equation method. For verification purposes, the results obtained with the new technique are successfully compared with examples taken from the literature. Complex antenna structures are then discussed in order to prove the usefulness of the new method.

**Citation:** Quesada-Pereira, F. D., A. Vidal, V. E. Boria, A. Alvarez-Melcón, and B. Gimeno (2007), Wavelet-like efficient analysis of two-dimensional arbitrarily shaped radomes using a surface formulation, *Radio Sci.*, *42*, RS5003, doi:10.1029/2006RS003522.

## 1. Introduction

[2] Radomes made of lossy dielectric layered materials, including antenna reflectors and feeding sources, are scattering problems whose accurate solution is typically difficult to compute, mainly due to their large size and complex geometries. For these reasons, it is a topic of growing interest which is presently receiving considerable attention by the electromagnetic community [see *Zhao et al.*, 2005; *Sukharevsky et al.*, 2005].

[3] Traditionally, radomes were first analyzed using high frequency methods, such as Ray Propagation in *Gao and Felsen* [1985], or the Geometrical Theory of Diffraction in *Duan et al.* [1991]. Alternatively, rigorous solutions for 2-D problems including canonical reflectors and radomes, combined with complex sources, were employed in *Chang and Chan* [1990], *Svezhentsev et al.* [1995], *Yurchenko et al.* [1999], *Oguzer* [2001], and *Oguzer et al.* [2004]. Although with reduced complexity, the scattering analysis of 2-D structures finds useful applications, for instance in the design of inductive or capacitive waveguide filters widely used in mobile and satellite systems. For these devices, the analysis can be carried out by solving a 2-D scattering problem. Also, cylindrical reflector antennas, which can be modeled as 2-D structures, are used in airborne navigation applications, as recognized in *Nosich* [1999]. These applications show the interest of investigating efficient numerical techniques for the study of 2-D scattering problems.

[4] Recently, solutions for 3-D radomes without reflectors based on volume and surface formulations have also appeared in *Lu* [2003] and *Zhao et al.* [2005], where the analysis has been performed through the Adaptive Integral Method [see *Zhao et al.*, 2005], and the Multilevel Fast

[1]Departamento de Tecnologías de la Información y las Comunicaciones, Technical University of Cartagena, Cartagena, Spain.
[2]Departamento de Comunicaciones, Universidad Politécnica de Valencia, Valencia, Spain.
[3]Departamento de Física Aplicada y Electromagnetismo-I.C.M.U.V., Universidad de Valencia, Valencia, Spain.


0048-6604/07/2006RS003522$11.00

Multipole Algorithm proposed in *Li and Li* [2004] and *Lu* [2003]. These 3-D radomes, typically used for fixed earth stations, usually present a spherical geometry. However, several cylindrical scenarios with arbitrary geometries appear in naval radar systems [see *Nosich*, 1999], as well as in telecommunications towers with radiant elements. In these complex real situations, multilayered radome materials are used, and metallic surfaces and reflectors combined with directive complex sources are often found in practice.

[5] In this paper, we propose to use the Equivalence Principle in order to formulate an integral equation problem for the analysis of 2-D cylindrical problems with arbitrary geometries. To set up the formulation we employ the Extinction Theorem to transform the classical volume formulation for dielectric obstacles into a more efficient surface approach. Proceeding in this way, the unknowns of the problem are the equivalent electric and magnetic surface currents defined only over the surfaces of the different homogeneous objects. Therefore, following this approach, a boundary integral equation fully characterizes the problem. That approach was already proposed in *Arvas and Ponnapalli* [1989] for small radomes scattering problems, and a more complete formulation for considering thin dielectric radomes under $\mathbf{TE}^z$ polarization was presented in *Sadigh and Arvas* [1992]. In this paper, a Poggio Miller Chang Harrington Wu Tsai (PMCHWT) field formulation of the type shown in *Kishk and Shafai* [1986] for large dielectric radomes under $\mathbf{TM}^z$ and $\mathbf{TE}^z$ polarization, including also metallic reflectors and complex sources, will be proposed. Furthermore, we have successfully combined such new formulation with the wavelet-like transform. If high accuracy is demanded, then the number of unknowns grows even in the case of surface formulations [see *Peterson et al.*, 1998]. That is the case, for instance, if a simple point-matching Method of Moments (MoM) procedure is used to solve the problem involving electrically large radomes, and/or very complex geometries. Then, CPU cost becomes important, and the wavelet-like transform can be efficiently used to decrease the amount of required memory allocation and CPU computational time.

[6] The use of wavelets to reduce the computational burden associated to MoM solutions is not new, and the idea has been used for instance in *Wang* [1995] to study the scattering from metallic objects. In that work periodic wavelet functions are used as basis functions in the MoM, and the backscattering of several metallic objects are successfully computed. Alternatively, in this paper we propose a surface formulation for the analysis of both metallic and dielectric objects, with subsequent application of the wavelet-like transform. Following this approach, the MoM formulation stays very simple (pulse-point matching), while obtaining big gain in computational cost through the use of the wavelet-like transform.

[7] It will also be shown in this paper that the use of the proposed surface formulation is very convenient for speed acceleration, since it leads to a matrix equation which naturally has a banded submatrix-type structure. This banded structure is very well suited for a subsequent introduction of the wavelet-like transform. An important contribution of this paper is that the wavelet-like transform is applied to each submatrix block, instead of using a global transformation scheme. It has been proved that a considerable gain in computational cost is obtained when the wavelet-like transform is applied following the new introduced subblock scheme. All these gains in CPU time and memory requirements are not possible if other volume based formulations [see *Hsu and Auda*, 1986; *Lu*, 2003; *Sukharevsky et al.*, 2005] are employed. This is because a volume formulation produces full dense matrices, thus loosing some of the matrix sparsity introduced by the proposed surface formulation. Furthermore, the volume formulation presents problems associated to the sorting of the grid elements, which reduce the computation gain related to the application of the wavelet-like transform.

[8] The structure of this paper is the following one. First, the surface formulation employed is briefly described. Then, the wavelet-like transformation is applied in order to obtain very sparse matrices. The theory is validated with general results obtained from the literature, such as canonical reflectors and radomes. Once the novel method is successfully verified, it has been applied to analyze complex shaped reflector-in-radome structures and arrays-in-radome antennas. The results clearly show the validity and usefulness of the new strategy proposed in this paper for the efficient and accurate analysis of this kind of structures.

## 2. Theory

[9] Let us consider a cylindrical radome problem like the one shown in Figure 1, where the radome can be composed of a multilayered dielectric and/or magnetic media with losses. We will consider that the dielectric permittivity and the magnetic permeability are defined as $\varepsilon_i = \varepsilon_0\varepsilon_{ri}$ and $\mu_i = \mu_0\mu_{ri}$ respectively. We assume that a $\mathbf{TM}^z$ or $\mathbf{TE}^z$ polarization can be selected as the excitation for the $n$ complex sources situated in the innermost layer, where a Perfect Electric Conductor (PEC) may also be present for modeling typically a reflector placed inside the antenna structure.

[10] First, we will set up the integral equations that arise for such problem following an equivalent surface formulation, and then the wavelet-like transform will be introduced to increase the computational efficiency of the analysis technique.

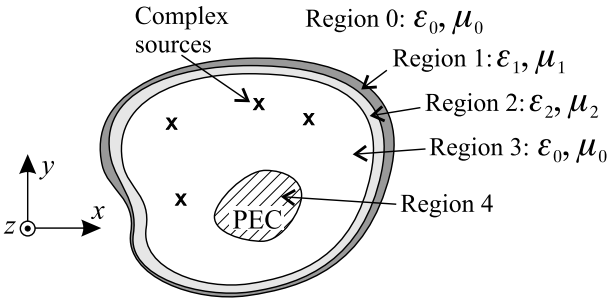


**Figure 1.** Scattering of lossy dielectric and magnetic multilayered radome with complex sources excitation including the presence of a metallic obstacle, under 2-D $\mathbf{TM}^z$ or $\mathbf{TE}^z$ excitation.

### 2.1. Equivalent Surface Formulation

[11] The scattering of homogeneous material bodies can be efficiently accomplished by using the Surface Equivalence Principle described in *Balanis* [1989] and *Chen* [1989]. Following this technique, the scattered fields in each region of the problem are due to equivalent electric and magnetic surface current densities ($\vec{J}(\vec{\rho}')$, $\vec{M}(\vec{\rho}')$), and can be expressed as follows:

$$\vec{E}_i^s(\vec{\rho}) = -j\omega\vec{A}_i(\vec{\rho}) - \nabla V_i(\vec{\rho}) - \frac{1}{\epsilon_i}\nabla \times \vec{F}_i(\vec{\rho}) \qquad (1)$$

$$\vec{H}_i^s(\vec{\rho}) = -j\omega\vec{F}_i(\vec{\rho}) - \nabla U_i(\vec{\rho}) + \frac{1}{\mu_i}\nabla \times \vec{A}_i(\vec{\rho}) \qquad (2)$$

where the mixed potential representation for the fields has been used, and the index ($i$) stands for each region in the structure (see Figure 1). For a two dimensional problem, the Green's functions used in the kernel of the integral equation takes the following form:

$$G_i(\vec{\rho}, \vec{\rho}\,') = \frac{1}{4j} H_0^{(2)}(k_i|\vec{\rho} - \vec{\rho}\,'|) \qquad (3)$$

[12] The application of the equivalence principle to a homogeneous body leads to four different integral equations, two involving the electric field (one for the interior problem and one for the exterior problem), and the other two involving the magnetic field. However, there are only two unknowns associated to the previous four integral equations, namely the equivalent electric and magnetic current densities defined on the surface of the body. Consequently, different combinations are possible for the formulation of the final scattering problem. If we choose the two equations involving only the electric field, then the E-field formulation is obtained. On the contrary, we may select the two equations involving the magnetic field, therefore leading to the H-field formulation. It is known that the previous two formulations exhibit numerical difficulties at certain frequencies, corresponding to the natural resonances of the interior body [see *Peterson et al.*, 1998]. To avoid this undesired numerical behavior, one has to combine the electric and magnetic field integral equations in a precise way. Three other different formulations are obtained in this manner, namely the combined or C-field, the so called PMCHWT formulation proposed in *Poggio and Miller* [1973], and the Müller formulation [see *Müller*, 1969]. The combined or C-field strategy formulates one equation for the exterior problem, by using a linear combination of the corresponding electric and magnetic field equations. In a similar way, the second equation is obtained by linear combination of the electric and magnetic field equations of the interior problem. On the other hand, the PMCHWT formulation is based on the direct imposition of the continuity of the tangential electric and magnetic field through the scatterer contour. Therefore, the first equation is obtained with the imposition of the continuity of the electric field, while the second equation is obtained through the imposition of the continuity of the magnetic field across the boundary. Finally, the Müller formulation is based on the PMCHWT formulation, with the introduction of a slight modification. In this case, the interior and exterior fields are scaled by the corresponding constitutive parameters, before imposing the field continuity. Either the PMCHWT or Müller formulations avoid the problem of the internal resonances, as recognized in *Mautz and Harrington* [1979]. In this work we have employed the PMCHWT alternative, which requires the imposition of the following two boundary conditions:

$$\hat{n} \times \vec{E}_i^s = \hat{n} \times \vec{E}_{i+1}^a \qquad (4)$$

$$\hat{n} \times \vec{H}_i^s = \hat{n} \times \vec{H}_{i+1}^a \qquad (5)$$

where superscript ($s$) stands for scattered field, ($a$) for the total field that may contain an excitation component, and $\hat{n}$ is the outgoing normal unitary vector to the surface at each point on the contour (see Appendix A for details).

[13] The imposition of the appropriate boundary conditions leads to a system of coupled integral equations, which is solved by the well-known Method of Moments (MoM). The unknown equivalent electric and magnetic current densities have been expanded in terms of pulse basis functions, whereas delta functions have been employed for testing (Point-Matching). The theory of the complex sources to include directionality in point sources has been used. This complex source model is a

simple way to simulate the aperture width of a realistic horn feed, since an omnidirectional source in complex space is a beam source in real space [see *Suedan and Jull*, 1991]. In this case, the complex center of the point sources is defined as follows:

$$\vec{\rho}_s = \vec{\rho_0} + j\,b\,(\cos\beta\,\hat{x} + \sin\beta\,\hat{y}) \tag{6}$$

where $\vec{\rho}_0$ is the actual point source center, $b$ determines the source directivity, and $\beta$ is the beam pointing direction measured from the $\hat{x}$ axis [see *Oguzer et al.*, 1995; *Suedan and Jull*, 1991]. It is also known that the complex source beam is gaussian near its axis, as it happens for the main beams of most realistic antennas [see *Suedan and Jull*, 1991]. By properly adjusting both the directivity and the beam pointing direction, it is easy to model more realistic feeding structures for reflector antennas, such as horns or arrays.

[14] The scattering of an object composed of $N$ nested homogenous layers is appropriately formulated on the outer contour of each layer. Once the standard Point-Matching method is applied to the numerical solution of the integral equation (see more details in *Arvas and Ponnapalli* [1989]), a banded MoM matrix of the following form is obtained,

$$\mathbf{Z}\cdot\mathbf{I} = \mathbf{V} \tag{7}$$

where the known voltage vector $\mathbf{V}$ directly depends on the modal excitation in (4) and (5), and the current vector $\mathbf{I}$ represents the unknown expansion coefficients of the basis functions for the electric and magnetic current [see *Peterson et al.*, 1998]. These previous vectors adopt the following general structure:

$$\mathbf{I} = \begin{bmatrix} \mathbf{I}^1_{JM} \\ \mathbf{I}^2_{JM} \\ \vdots \\ \vdots \\ \mathbf{I}^N_{JM} \end{bmatrix}, \mathbf{V} = \begin{bmatrix} \mathbf{V}^1_{EH} \\ \mathbf{V}^2_{EH} \\ \vdots \\ \vdots \\ \mathbf{V}^N_{EH} \end{bmatrix}. \tag{8}$$

[15] Finally, the impedance matrix $\mathbf{Z}$ is the standard MoM matrix obtained from the overlapping integrals between the Green's functions (3) and the selected basis and test functions, as proposed in *Peterson et al.* [1998]. For the case of $N$-nested layers, treated with the surface integral equation, this impedance matrix can be further decomposed into the following subblock structure:

$$\mathbf{Z} = \begin{bmatrix} \mathbf{Z}^{11} & \mathbf{Z}^{12} & 0 & \cdots & 0 \\ \mathbf{Z}^{21} & \mathbf{Z}^{22} & \ddots & \ddots & \vdots \\ 0 & \ddots & \ddots & \ddots & 0 \\ \vdots & \ddots & \ddots & \mathbf{Z}^{(N-1)(N-1)} & \mathbf{Z}^{(N-1)N} \\ 0 & \cdots & 0 & \mathbf{Z}^{N(N-1)} & \mathbf{Z}^{NN} \end{bmatrix} \tag{9}$$

[16] As it can be seen in (9), the sparsity of this matrix grows with the number of layers ($N$). This fact, together with the wavelet-like transform proposed in this paper, reduces the computational time and also the memory requirements of the problem.

[17] Each of the submatrices $\mathbf{Z}^{QP}$ of the impedance matrix (9) can be further decomposed into four submatrices, each one representing the electric or magnetic fields imposed on the $Q$ layer contour, caused by the equivalent magnetic or electric current surface densities that flow on the contour $P$:

$$\mathbf{Z}^{QP} = \begin{bmatrix} \mathbf{Z}_{E_Q J_P} & \mathbf{Z}_{E_Q M_P} \\ \mathbf{Z}_{H_Q J_P} & \mathbf{Z}_{H_Q M_P} \end{bmatrix} \tag{10}$$

[18] If the innermost layer $N$ is a PEC, the expression of the interaction matrices is slightly different due to the lack of magnetic current density. In that case, the submatrix $Z^{NN}$ presents a single subblock structure, and the matrices involving the sub-indexes $N$ and $(N-1)$ contain only the corresponding 2 appropriate subblocks. Consequently, the sub-vector $\mathbf{I}^N_{JM}$ does only include the electric surface current, and $\mathbf{V}^N_{EH}$ considers the corresponding boundary conditions for the metallic surface. In the case of a closed metallic object a combined field approach is used. This is done by introducing in the integral equations a new parameter $\alpha$ suggested in *Peterson et al.* [1998] (see Appendix A for details). This parameter combines the EFIE and MFIE formulation for a conductor, thus avoiding again the internal resonance problem:

$$\mathbf{Z}^{NN} = [\alpha\mathbf{Z}_{E_N J_N} + (1-\alpha)\mathbf{Z}_{H_N J_N}] \tag{11}$$

$$\mathbf{Z}^{(N-1)N} = \begin{bmatrix} \mathbf{Z}_{E_{N-1} J_N} \\ \mathbf{Z}_{H_{N-1} J_N} \end{bmatrix} \tag{12}$$

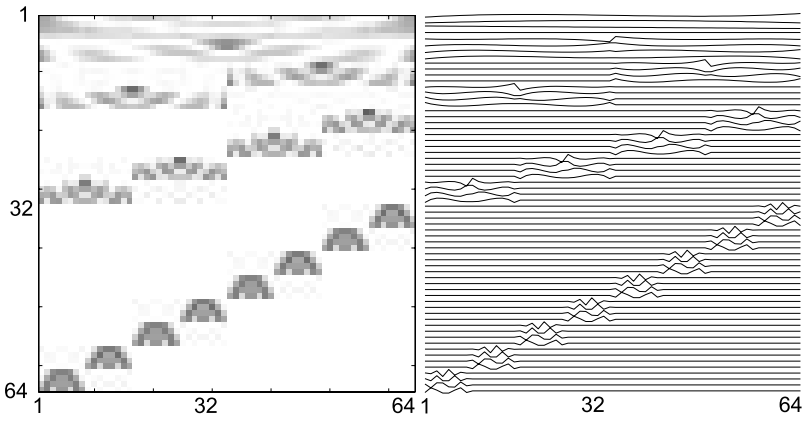


**Figure 2.** An example of a wavelet-like transformation matrix **T** with order $k = 4$ and $M_s = 64$ showing the basis vectors.

$$\mathbf{Z}^{N(N-1)} = \alpha[\mathbf{Z}_{E_N J_{N-1}}\ \mathbf{Z}_{E_N M_{N-1}}] + (1-\alpha)[\mathbf{Z}_{H_N J_{N-1}}\ \mathbf{Z}_{H_N M_{N-1}}] \tag{13}$$

[19] In the above equations, $\alpha$ is selected between zero and one, depending on the weight given to each electric or magnetic type integral equation. For the problems investigated in this paper we have used a value of $\alpha = 0.05$ in order to give some importance to the MFIE, thus avoiding resonance effects of the EFIE described in *Davis and Warnick* [2005].

[20] The proposed impedance matrix presents many submatrices that are systematically set to zero, since there are no interactions between noncontiguous layers, as it can be seen in (9).

### 2.2. Wavelet Transform

[21] The next stage in the solution of the coupled integral equations system is the use of the wavelet transform. Wavelet bases may be applied in two different ways when solving integral equations through the MoM. The most rigorous approach consists on considering the wavelet family as base and test functions in the MoM implementation [see *Steinberg and Leviatan*, 1993], thus typically involving major computational efforts. An alternative strategy, which consists on applying a wavelet matrix transformation to the matrix arisen from the conventional application of the MoM, has been recently proposed in *Baharav and Leviatan* [1998], *Sarkar and Kim* [1999], and *Wagner and Chew* [1995]. In this paper, we have followed this second approach, which can improve the efficiency and the memory requirements when large matrices are involved in the numerical solution of the integral equation, as it typically happens when the objects are electrically large.

[22] In *Vidal et al.* [2004] and *Sarkar et al.* [2002], wavelet-like bases were proposed to reduce the CPU time and memory requirements related to the characterization of 2D large metallic objects. Due to such previous experiences, the study of the wavelet families has not been considered in this paper, and the wavelet-like family described in the previous references has instead been directly applied to our problem. Here, a brief description of the wavelet-like transform is given. The conversion of the discrete integral operator into the new wavelet-like bases is equivalent to carry out a similarity transformation. The similarity transformation matrix is defined by a real and unitary matrix, **T**, whose rows contain the new wavelet-like bases as described in *Alpert et al.* [1993] and *Vidal et al.* [2004]. The wavelet-like transformation matrix **T** is built from the discretization grid $S = \{x_1, x_2, \ldots, x_{Ms}\} \subset \mathbb{R}$. Then, an orthonormal basis for the $M_s$-dimensional space of functions defined on $S$ is constructed following *Alpert et al.* [1993]. We assume that $M_s = 2^n \cdot k$, where $n$ is an integer and $k$ is the wavelet-like order. The basis vectors present some fundamental properties: all but $k$ basis vectors have $k$ vanishing moments, they preserve the condition number of the full matrix and they present local support. Therefore, they provide a multiresolution representation, although they are not strictly dilations and translations of a mother function like a conventional wavelet scheme. Instead, the basis vectors are obtained by a number of Gram-Schmidt orthogonalizations starting from polynomials based on $S$ (see *Alpert et al.* [1993] for details). The transformation matrix **T** with its corresponding basis vectors are shown in Figure 2 for an example of an equidistant grid $S$ with $M_s = 64$ and $k = 4$.

[23] The application of the wavelet-like method can increase the sparsity of the original matrix **Z** (that contains $M^2$ elements including zero entries) shown in (9). So, an

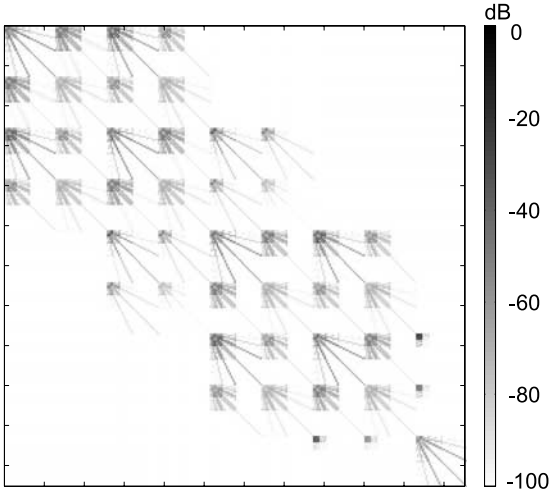


**Figure 3.** Matrix $\tilde{\mathbf{Z}}$ after thresholding for the sandwiched radome for the broadcasting tower taken from section 3.2, with $\mathbf{TE}^z$ incidence and threshold equal to 0.5%.

iterative sparse algorithm can be used to solve the new problem with complexity $O(M')$, where $M'$ is the number of nonzero elements in the sparse impedance matrix that should be much lower than $M^2$. This strategy compares very favorably to the $O(M^3)$ operations that requires the direct solution of the original problem using a standard LU decomposition, or to the $O(M^2)$ operations that needs an iterative solver that also depends on the condition number of the matrix.

[24] The wavelet-like transform could directly be applied to the complete matrix at once. However, the numerical results obtained have revealed that much better results are obtained for a subblock wavelet transform. The idea of applying the wavelet transform, following a subblock scheme, to the impedance matrix resulting from the application of the surface formulation to radome problems is an important contribution of this work, not explored before to the authors' knowledge. As an example, the overall computational cost of the solution using wavelet-like approach applied in one block to the $\mathbf{Z}$ matrix takes 5 times more operations, leading to a much less sparse matrix (80% versus 95%) than the subblock decomposition proposed in this paper. The selected problem to perform this comparative evaluation is the broadcast square tower with circular sandwiched radome described in section 3.2. Nevertheless, sparsity gains due to this subblock scheme have been also observed for all the examples considered in this paper, which are more impressive when the number of layers grows. When applying the wavelet transform to each subblock, we must consider that all the submatrices are not square. This is due to the fact that each contour needs a different number of discretization segments, therefore requesting a different transformation matrix $\mathbf{T}_P$ for each layer $P$. The original problem is now represented, in the wavelet-like domain, as follows:

$$\tilde{\mathbf{Z}}\tilde{\mathbf{I}} = \tilde{\mathbf{V}} \tag{14}$$

$$\tilde{\mathbf{Z}}^{QP} = \begin{bmatrix} \mathbf{T}_Q \mathbf{Z}_{E_Q J_P} \mathbf{T}_P^t & \mathbf{T}_Q \mathbf{Z}_{E_Q M_P} \mathbf{T}_P^t \\ \mathbf{T}_Q \mathbf{Z}_{H_Q J_P} \mathbf{T}_P^t & \mathbf{T}_Q \mathbf{Z}_{H_Q M_P} \mathbf{T}_P^t \end{bmatrix} \tag{15}$$

$$\tilde{\mathbf{I}}_{JM}^P = \begin{bmatrix} \mathbf{T}_P \mathbf{J}_P \\ \mathbf{T}_P \mathbf{M}_P \end{bmatrix} \tag{16}$$

$$\tilde{\mathbf{V}}_{EH}^Q = \begin{bmatrix} \mathbf{T}_Q \mathbf{E}_Q \\ \mathbf{T}_Q \mathbf{H}_Q \end{bmatrix} \tag{17}$$

where superscript ($t$) stands for the transpose of a matrix, and the tilde indicates that the matrices are expressed in the new wavelet-like bases. Due to the wavelet-like bases properties, $\tilde{\mathbf{Z}}$ presents many negligible elements that are set to zero through a hard threshold applied to each one of the submatrices of $\tilde{\mathbf{Z}}$. This last operation completes the subblock transformation scheme proposed in this paper.

[25] However, the wavelet approach involves matrix and vector transformations, whose cost should be included within the global computational budget. The wavelet-like transform of a submatrix can be evaluated in $O(M_s^2)$ operations [see *Vidal et al.*, 2004; *Sarkar et al.*, 2002], where $M_s$ is the number of unknowns for that submatrix. This operation should be carried out for the $(12N - 15)$ submatrices that compose the total matrix $\mathbf{Z}$ in the case of $N$-layers, including a final metallic object. For that reason, this extra computation cost has been considered in all the validation results.

[26] The transformed impedance matrix presents a diagonal banded form usually known as finger structure, as it can be seen in Figure 3 for the broadcast square tower with circular sandwiched radome described in section 3.2.

## 3. Validation Results

[27] In this section, several practical nonmagnetic radome designs taken from the literature have been successfully considered. Some of them could be analyzed following the approximate technique for electrically thin radomes proposed in *Sadigh and Arvas* [1992]. However, the more accurate formulation described in this paper has been employed in all the examples, since it can

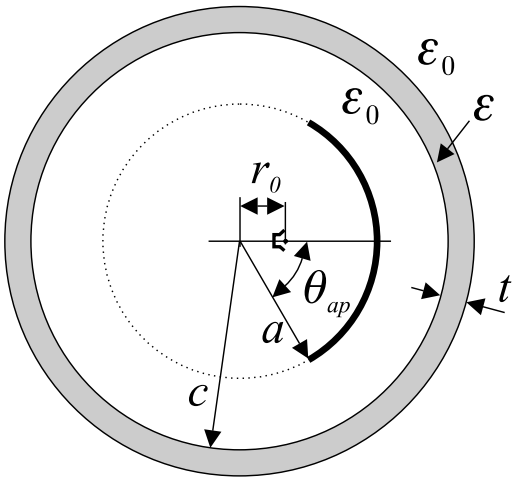


**Figure 4.** Circular dielectric 2-D radome ($\varepsilon = \varepsilon_r\varepsilon_0$) with a complex source excitation, including a concentric circular metallic reflector.

also be applied to thick radomes as well a considering the possible use of magnetic materials.

[28] All the examples considered in this section contain elements with large physical dimensions. As a consequence, big computational savings can be obtained when using the proposed wavelet-like approach. A wavelet-like family of 8 vanishing moments has been considered for all the examples, and ten points per free space wavelength are used for discretization. The efficiency study compares the number of floating point operations (Mflops) required by each method including the wavelet-like transform, using a standard command provided by the commercial software *Matlab©*. The threshold value has been adapted to the geometry of each problem for the maximum computational gain, considering a certain low error that preserves the normalized field when compared with the conventional MoM solution.

### 3.1. Circular Radome and Circular Reflector

[29] The first example has been taken from *Svezhentsev et al.* [1995]; the geometry is shown in Figure 4. The data for this reflector are $\varepsilon_r = 4$, $c = 15.915\ \lambda$, $a = 9.995\ \lambda$, $r_0 = a/2$, $b = 0.796\ \lambda$, $t = 0.22\ \lambda$ and $\theta_{ap} = 30°$. The size of this structure is considerably large, since the circular radome presents two contours of approximately $100\lambda$ of perimeter.

[30] The normalized electric fields obtained with the original and the wavelet-like implementation are both presented in Figure 5 for $\mathbf{TM}^z$ polarization, where the radiation pattern of the antenna without radome is also shown for comparative purposes. The electric field also compares very well with the same example solved with a different method in *Svezhentsev et al.* [1995]. Furthermore, the wavelet-like transform introduces strong savings in CPU cost, preserving at the same time the radiation pattern, where only small errors are observed for very low sidelobe levels. The sparsity achieved in this example reaches 83.4%, and the computational cost is 3.7 times lower than the one required by the direct MoM

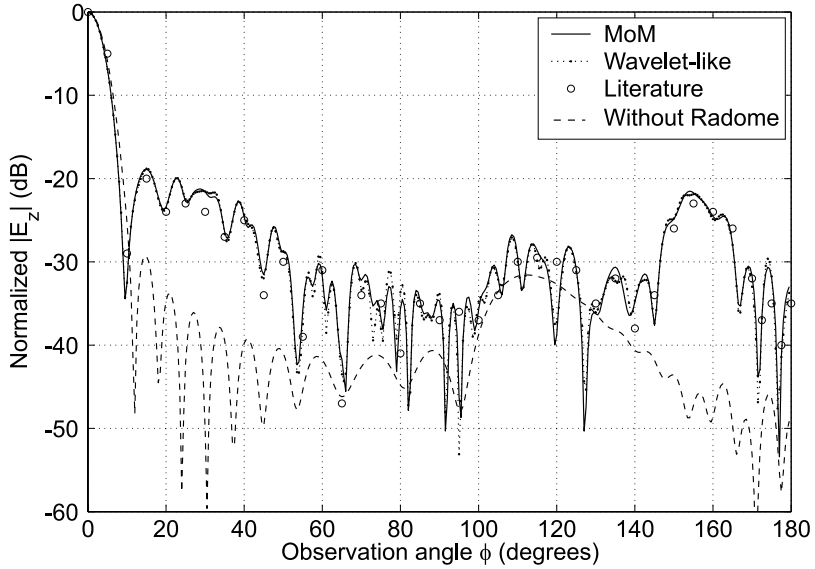


**Figure 5.** Normalized electric field under $\mathbf{TM}^z$ polarization, for the structure shown in Figure 4. (In the legend, literature refers to data taken from *Svezhentsev et al.* [1995].)

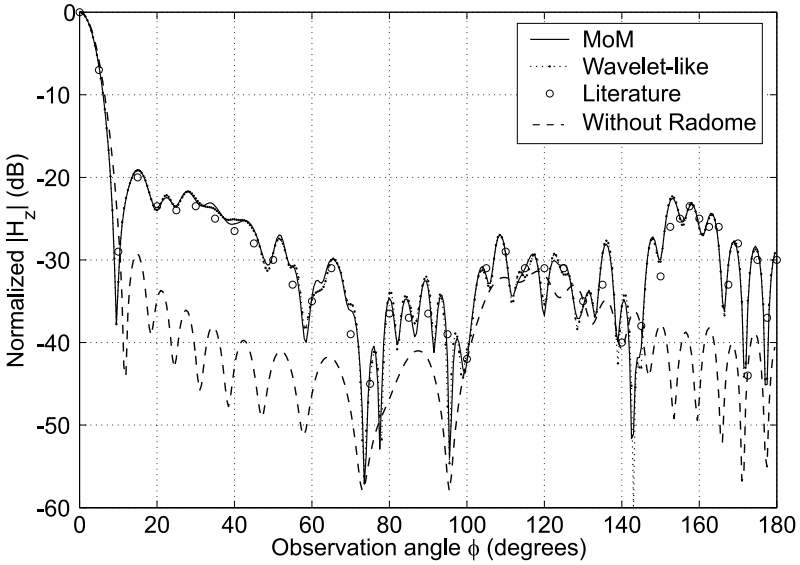


**Figure 6.** Normalized magnetic field under $\mathbf{TE}^z$ polarization, for the structure shown in Figure 4. (In the legend, literature refers to data taken from *Svezhentsev et al.* [1995].)

method, for a relative mean square error of 0.04%, and using a threshold level of 0.2%. The error has been defined as the relative mean square difference between the original MoM field and the wavelet-like MoM one.

[31] The normalized magnetic fields obtained with the original MoM method and the wavelet-like implementation are successfully compared in Figure 6, in this case for $\mathbf{TE}^z$ polarization. The radiation pattern of the antenna without radome has been also shown for comparative purposes. The magnetic field provided by the wavelet-like implementation also compares very well in this case with the results given by the method proposed in *Svezhentsev et al.* [1995]. In this second example, the wavelet-like transform achieves 78% of matrix sparsity, and the computational cost is 3.3 times lower than the effort required by the direct MoM solution, for a relative mean square error of 0.02%, and using a threshold level of 0.07%.

[32] The next example was originally reported in *Yurchenko et al.* [1999], with the geometry detailed in Figure 7. The relevant dimensions in this case are: $L = 4.271\ \lambda$, $\varepsilon_r = 2$, $c = 5.984\ \lambda$, $a = 4.997\ \lambda$, $r_0 = 0.56a$, $b = 0.414\ \lambda$, $t = 0.241\ \lambda$ and $\theta_{ap} = 30°$. The normalized magnetic field obtained with the original and the wavelet-like implementation are both presented in Figure 8 for $\mathbf{TE}^z$ polarization. The magnetic field again compares very well with the same example solved with a different method in *Yurchenko et al.* [1999]. In this case, the wavelet-like transform achieves 91% of matrix sparsity, and the computational cost is 7.3 times lower than the direct method, for a very low relative mean square error of 0.006%, and using a threshold of 0.08%. Again, this error has been defined by comparing the original MoM and the wavelet-like MoM.

[33] In addition to the scattering behavior of the structure shown in Figure 7 at a given frequency, we have investigated the accuracy and numerical stability of the technique when the thickness of the radome increases. Figure 9 shows the normalized radiated power as a function of the radome thickness, while Figure 10

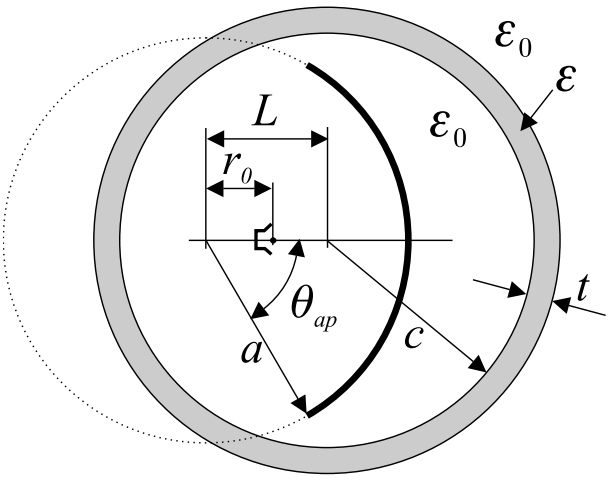


**Figure 7.** Circular dielectric 2-D radome ($\varepsilon = \varepsilon_r \varepsilon_0$) with a complex source excitation, including a noncon-centric circular metallic reflector.

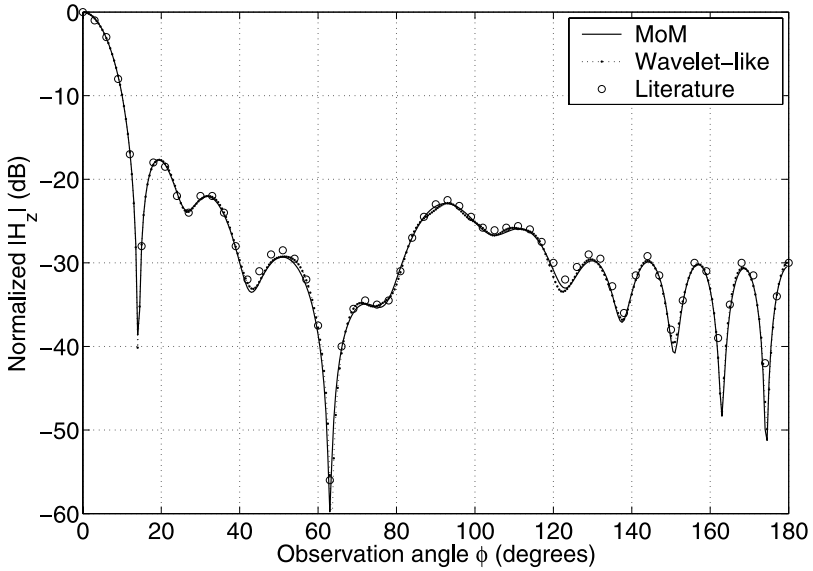


**Figure 8.** Normalized magnetic field under $\mathbf{TE}^z$ polarization for the example shown in Figure 7. (In the legend, literature refers to data taken from *Yurchenko et al.* [1999].)

shows the directivity. Results reported in *Yurchenko et al.* [1999] are shown for validation purposes. We can observe in the figure very good agreement with our technique, both for the radiated power and for the directivity, and in the whole range of dimensions considered.

[34] The agreement obtained in the above example is very good since there are no natural resonances of the

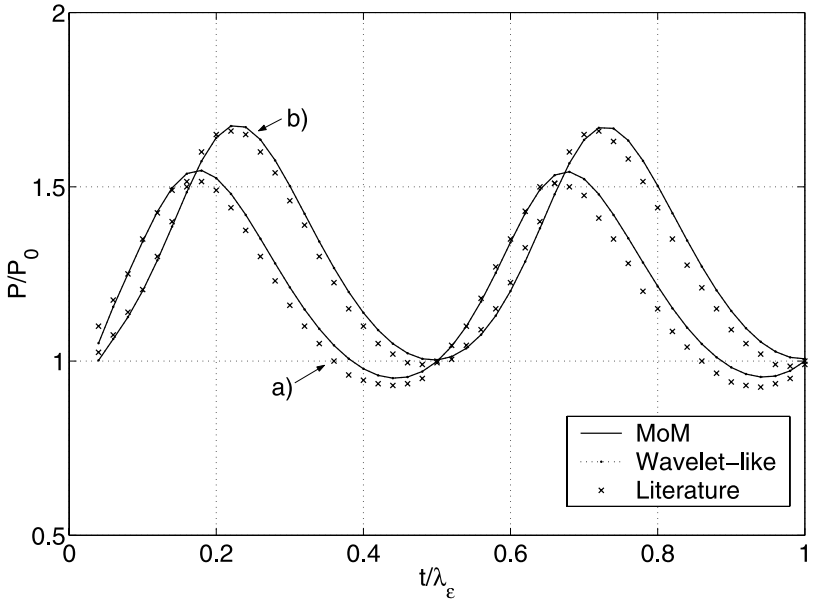


**Figure 9.** Normalized total radiation power as function of the radome thickness $t$ for the structure shown in Figure 7. (a) $L = 4.271\ \lambda$, $c = 5.984\ \lambda$, $r_0 = 0.56\ a$, and (b) $L = 4.330\ \lambda$, $c = 6.0\ \lambda$, $r_0 = 0.533\ a$. In both cases, the remaining dimensions are the same ones used to obtain Figure 8 (literature refers to *Yurchenko et al.* [1999]).

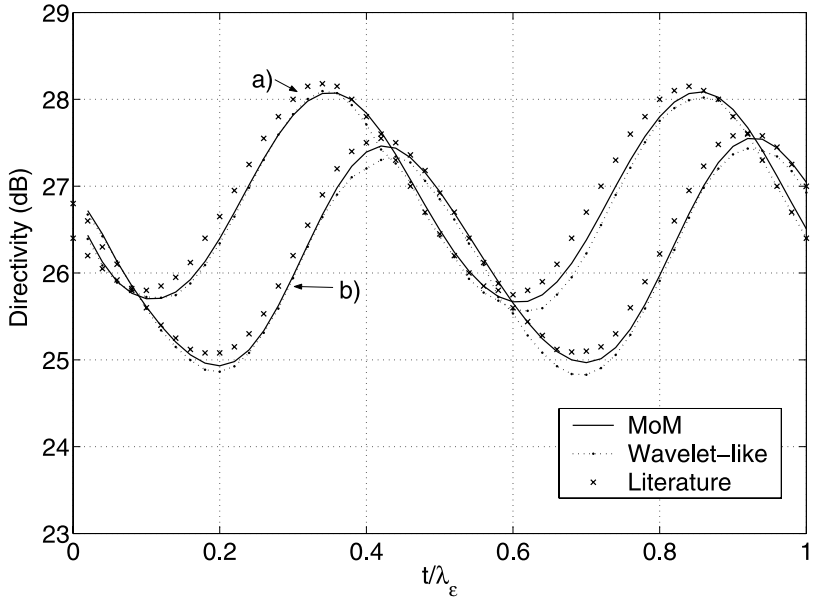


**Figure 10.** Directivity as function of the radome thickness $t$ for the example shown in Figure 7. (a) $L = 4.271\ \lambda$, $c = 5.984\ \lambda$, $r_0 = 0.56\ a$, and (b) $L = 4.330\ \lambda$, $c = 6.0\ \lambda$, $r_0 = 0.533\ a$. In both cases, the remaining dimensions are the same ones used to obtain Figure 8 (literature refers to *Yurchenko et al.* [1999]).

structure for the parameters studied. An interesting question that arises is how the developed IE surface technique behaves close to such resonances [see *Hower et al.*, 1993]. We have investigated this important issue for the example given in *Hower et al.* [1993], comparing the technique developed in this paper with a volume surface integral equation and an FDTD technique presented in *Hower et al.* [1993]. We have found that for a similar level of discretization, the surface integral equation leads to more accurate results than both the volume formulation and the FDTD technique. In particular we have checked that the surface formulation developed in this work is more accurate close to the natural resonances of the body. However, to maintain the same level of accuracy close to the resonance, we need around four times higher number of unknowns than for a region far from the resonance. Increasing the number of basis functions, then, assures a good convergence of the method even close to the natural resonances of the structure. Alternatively, in order to solve this convergence problem, a regularization technique proposed in *Nosich* [1999] can be employed to smooth the kernel of the integral equations close to singularities.

### 3.2. Circular Sandwich Radome Mounted on a Telecommunications Tower With Square Basis

[35] The next example is taken from the cylindrical geometry typically employed in broadcasting towers considering hard weather conditions [see *Sadigh and Arvas*, 1992]. This example involves several elements, including a sandwiched circular radome, as shown in Figure 11. In that case, the support of the tower is given by a fiberglass plastic reinforced radome that presents three layers. The core of low relative dielectric permit-

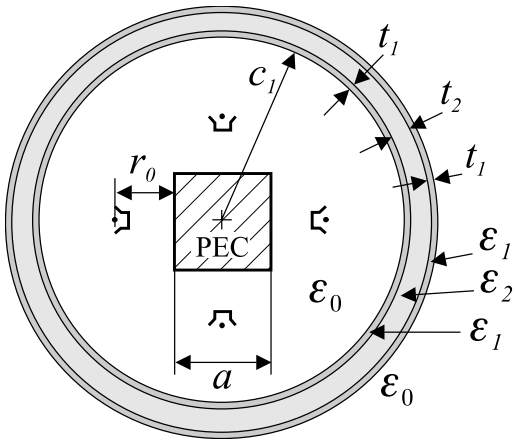


**Figure 11.** Circular dielectric 2-D radome with four complex source points and a square metallic base. The dimensions are: $t_1 = 1.8$ mm, $t_2 = 37.5$ mm, $c_1 = 0.82$ m, $a = 0.41$ m, $r_0 = 93.7$ mm, $\varepsilon_{r1} = 4.7(1 - j\,0.018)$ with $\varepsilon_1 = \varepsilon_{r_1}\varepsilon_0$, $\varepsilon_{r_2} = 1.07$ with $\varepsilon_2 = \varepsilon_{r_2}\varepsilon_0$.

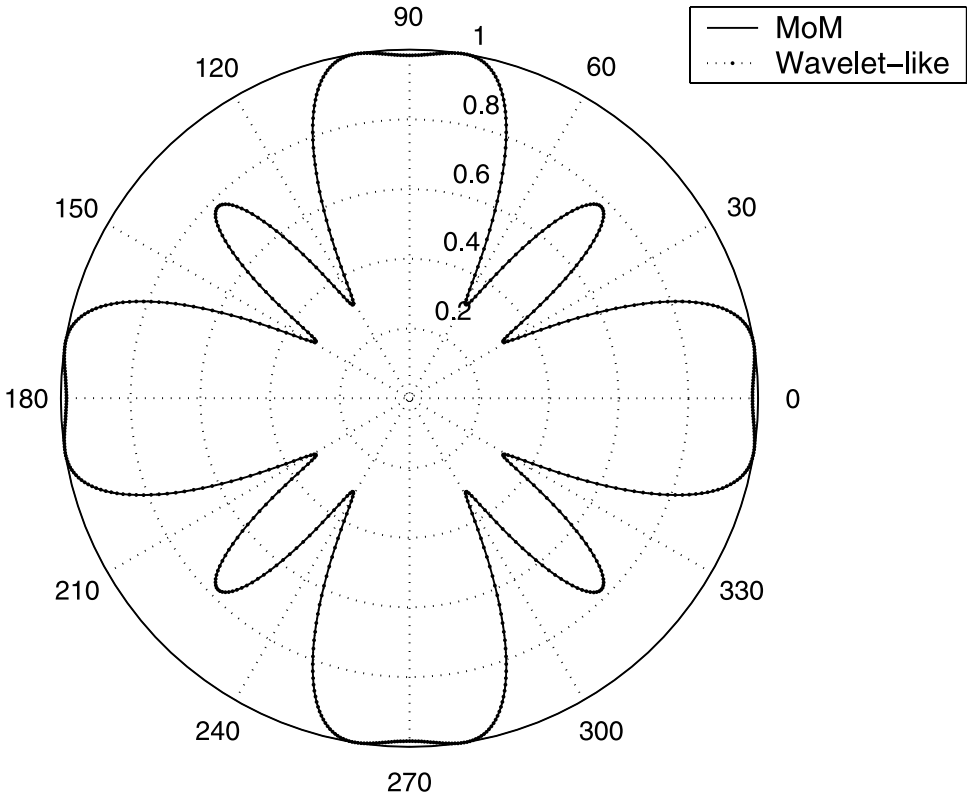


**Figure 12.** Normalized magnetic field produced by the structure shown in Figure 11. The results for the sandwiched radome obtained with direct MoM are shown with solid line, and the ones obtained with the wavelet-like solution are represented by dotted symbols.

tivity (foam) is made of a Rohacell® material, while the two side layers are made of thin fiberglass hard material, whose dielectric properties have been derived from the characteristics of a commercial fiber glass substrate, known as Pyrex®. The complex sources present an equivalent directivity of $k_0\, b = 2.6$, with $\mathbf{TE}^z$ polarization at a frequency of 800 MHz (UHF band). The complex sources model accurately the directivity and the radiation performance of the real wire antennas mounted on a telecommunications tower.

[36] In this analysis, we have first compared (see Figure 12) the solution given by the conventional MoM with the wavelet-like results. The agreement between both data is very good, achieving a 95% of matrix sparsity, and a computational cost reduction factor of 6, using a threshold of 0.5%. The resulting error in the normalized magnetic field reconstruction has been in this case very low (0.008%).

[37] In order to assess the influence of the sandwiched radome in the radiation pattern of a realistic telecommunication tower, we have analyzed the same structure shown in Figure 11 but with two different one-layer configurations. First, we have studied a radome composed only by the low permittivity foam material layer with its corresponding width $t_2$, whereas in the second case the layer is considered to be formed of a thin layer of fiberglass material of width $t_1$. In Figure 13, we can see a considerable increase in the sidelobe levels of the antenna when the radome is modified. These results clearly show that a careful design of the radome considering the three layers of material is needed if low sidelobe levels are requested in a practical application.

### 3.3. Half-Circular Dielectric Shell With Metallic Back Plate

[38] The following example considers a uniform phased array composed of 31 filaments, fed with cosine law amplitudes and with constant separation of 0.6 $\lambda$ with $\mathbf{TE}^z$ polarization. The array is located inside a half dielectric circular shell with a finite metallic back plate, as shown in Figure 14. A similar example was studied in *Sukharevsky et al.* [2005] with the only difference that an infinite metallic back plate was used. The normalized electric field is shown in Figure 15, where it is success-

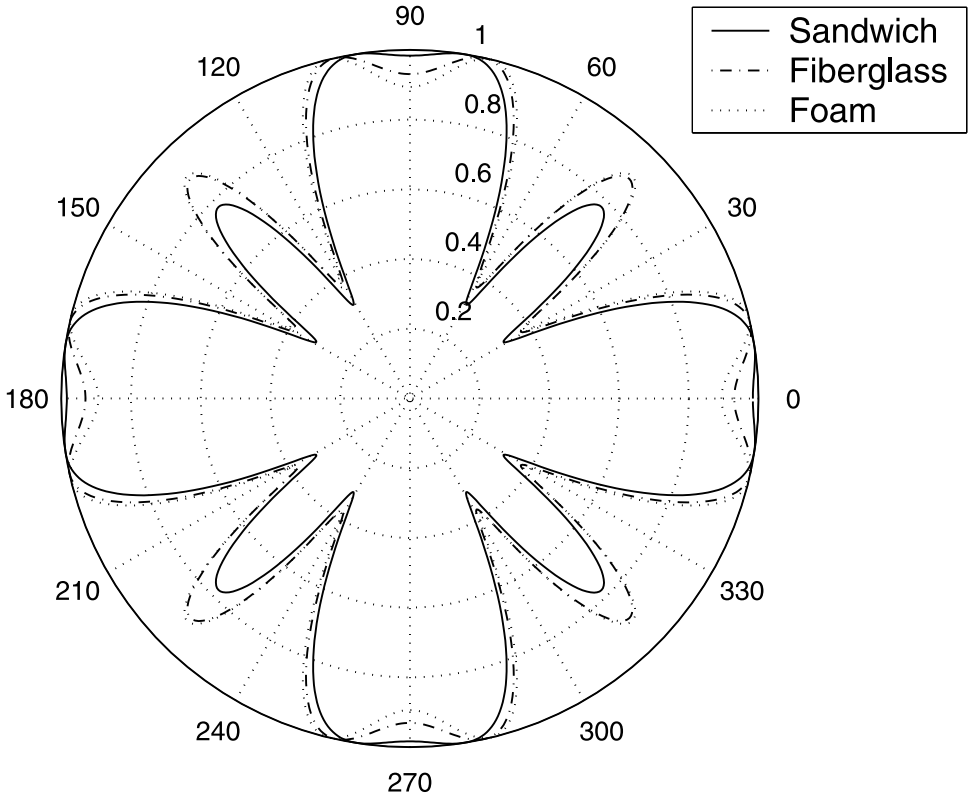


**Figure 13.** Normalized magnetic field produced by wavelet-like method for the original sandwiched radome (three layers) in solid line, and for two different simpler radomes. The dashed-dotted line shows the results obtained for a radome composed of only one layer of fiberglass material of width $t_1 = 1.8$ mm, while the dotted line shows the results when the single layer is made of foam with a width of $t_2 = 37.5$ mm.

fully compared with the analytical results given in *Sukharevsky et al.* [2005]. The results compare very well for observation angles from 0 to approximately 60, where the effects of the finite back plate geometry begin to be important in a realistic scenario. In this case, the wavelet-like matrix sparsity is of 89%, providing a reduction in computational cost of 6.8 using a threshold of 0.08%. The resulting error in the normalized electric field reconstruction has been of 0.03% when the wavelet-like technique is compared with the conventional MoM.

### 3.4. Ogive Radome With Parabolic Reflector

[39] An example considering a complex arbitrary radome surface is finally considered. A cylindrical parabolic reflector illuminated by a directive complex source with $\mathbf{TE}^z$ excitation is enclosed by an ogive-shaped radome. A similar problem has already been studied in *Kukobko et al.* [2005]. The simulated structure has not been optimized, since the objective is to show that its analysis is possible using the proposed technique. In our case, the

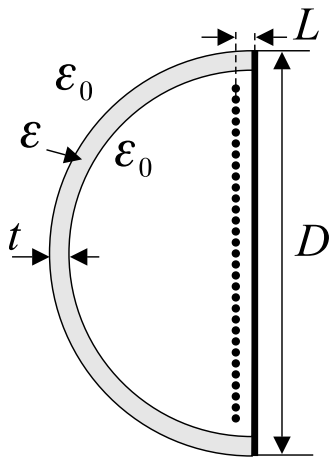


**Figure 14.** Dielectric half circular 2-D radome with a current array excitation and a back PEC finite plane. The dimensions are: $D = 22\ \lambda$, $t = 0.2\ \lambda$, $L = 0.25\ \lambda$ and $\varepsilon_r = 4$ with $\varepsilon = \varepsilon_r\varepsilon_0$.

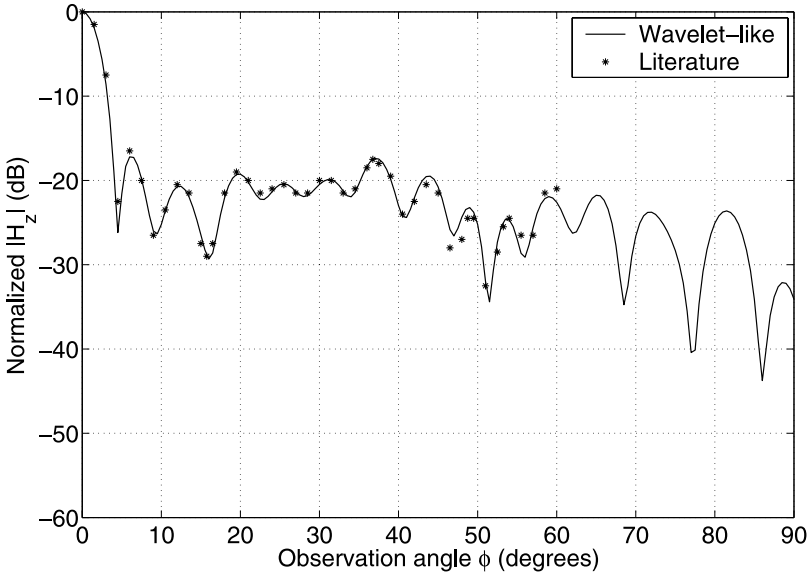


**Figure 15.** Normalized magnetic field obtained by the current array in the half-circular dielectric radome structure shown in Figure 14 (literature refers to *Sukharevsky et al.* [2005]).

parametric curve for the ogive is taken from the superspheroidal profile $y^2 = (D/2L)^2(L^\nu - x^\nu)^{2/\nu}$, with $\nu = 1.449$ [see *Zhao et al.*, 2005]. The analysis has been performed including a parabolic reflector with the geometry shown in Figure 16. The resulting normalized magnetic field is shown in Figure 17. In this example, the number of unknowns is 4224. The original sparsity before wavelet transformation is equal to 4.4%, and the transformed matrix sparsity is equal to 94.5%. The original computation cost is $195.5 \cdot 10^9$ floating point operations and the wavelet solution is achieved in $19.4 \cdot 10^9$ floating point operations, thus providing a reduction factor in computational cost of 10, using a threshold of 0.07%. The resulting error in the normalized magnetic field reconstruction has been of 0.01%. This last result shows the versatility of the technique implemented, which leads to low error levels and large computational savings even for very complex antenna-radome structures. Then, some useful radome features may be easily obtained. In this example, the boresight error has been evaluated for gimbal angles up to 40 degrees, obtaining 0.3 degrees of maximum absolute error.

[40] It is interesting to note the presence of a sharped nose in the considered ogive radome, which typically requires a finer meshing than the smoother boundaries in order to recover convergent results. This fact obviously involves additional CPU effort on the practical implementation of the proposed surface IE technique. In order to recover the convergent results shown in Figure 17, the authors have observed that the number of unknowns in the sharp nose must be at least 2 times higher than those required by the smoother sections.

## 4. Conclusions

[41] This paper presents a surface formulation MoM solution for cylindrical complex radomes composed of multilayered lossy dielectric material with arbitrary

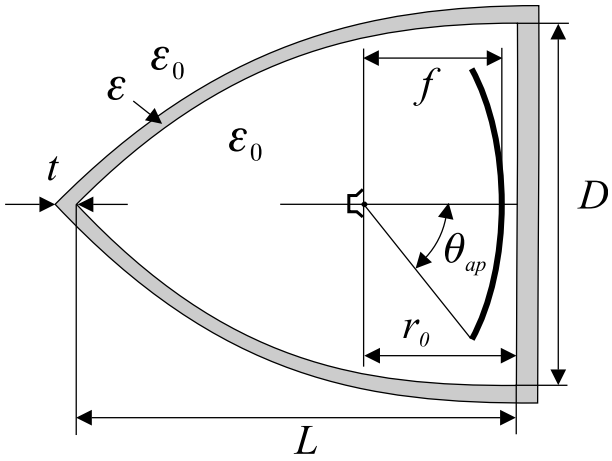


**Figure 16.** Dielectric 2-D radome with a complex source excitation and a parabolic metallic reflector. The dimensions are: $D = 12\ \lambda$, $L = 14\ \lambda$, $t = 0.125\ \lambda$, $f = 4\ \lambda$, $\theta_{ap} = 45$, $r_0 = 5.875\ \lambda$, $\varepsilon_r = 2$ with $\varepsilon = \varepsilon_r\varepsilon_0$ and $k_0 b = 2.6$.

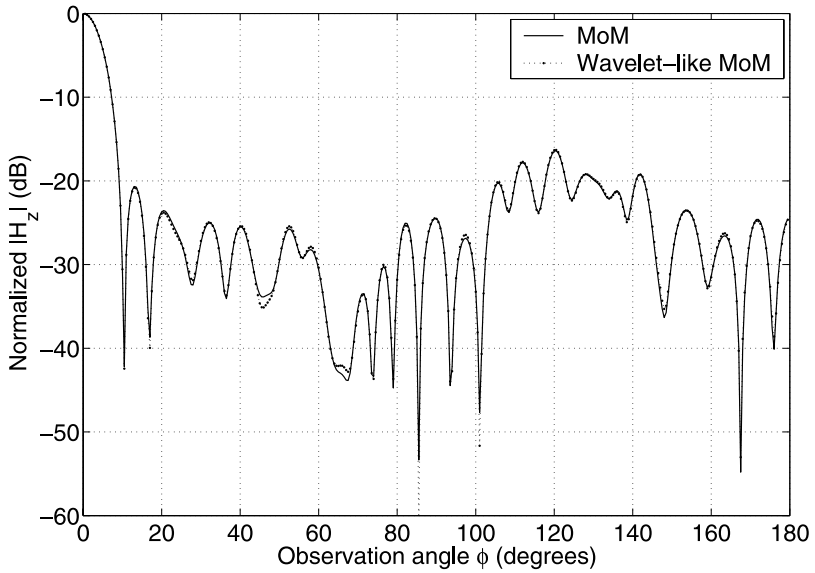


**Figure 17.** Normalized magnetic field obtained in the reflector-in-radome structure shown in Figure 16.

shape, arbitrary reflector surfaces, and directive complex sources. It provides an accurate and efficient method to study any type of large radome structure, thanks to the use of the wavelet-like transform. The use of a surface formulation together with the application of the wavelet-like transform following a subblock scheme, converts the original problem into a highly sparse one exhibiting a strong banded structure. Results are given showing the accuracy and efficiency of the technique even for very complex radome-antenna structures. Therefore, this approach opens the possibility for the analysis of large and complex antenna-in-radome structures using a conventional computer.

## Appendix A: Details of the Integral Equation

[42] The continuity relations for the tangent components of the fields across an interface between two different homogenous media (see (4) and (5)) can be expanded in terms of their mixed-potentials expressions (see (1) and (2)), and the Green's functions of a homogenous medium with constitutive parameters ($\epsilon_i$, $\mu_i$) (see (3)), yielding to a coupled system of integral equations, as follows:

$$\begin{aligned}
&\hat{n}\times\left\{\vec{E}_i^{(exc)}(\vec{\rho})-\frac{\omega\mu_i}{4}\int_C\vec{J}(\vec{\rho}\,')\,H_0^{(2)}(k_i|\vec{\rho}-\vec{\rho}\,'|)\,dC'\right.\\
&\quad-\frac{1}{4\omega\epsilon_i}\cdot\nabla\int_C\nabla'\cdot\vec{J}(\vec{\rho}\,')\,H_0^{(2)}(k_i|\vec{\rho}-\vec{\rho}\,'|)\,dC'\\
&\quad\left.-\frac{1}{4j}\nabla\times\int_C\vec{M}(\vec{\rho}\,')\,H_0^{(2)}(k_i|\vec{\rho}-\vec{\rho}\,'|)\,dC'\right\}=\\
&\hat{n}\times\left\{\vec{E}_{i+1}^{(exc)}(\vec{\rho})+\frac{\omega\mu_{i+1}}{4}\int_C\vec{J}(\vec{\rho}\,')\,H_0^{(2)}(k_{i+1}|\vec{\rho}-\vec{\rho}\,'|)\,dC'\right.\\
&\quad+\frac{1}{4\omega\epsilon_{i+1}}\cdot\nabla\int_C\nabla'\cdot\vec{J}(\vec{\rho}\,')\,H_0^{(2)}(k_{i+1}|\vec{\rho}-\vec{\rho}\,'|)\,dC'\\
&\quad\left.+\frac{1}{4j}\nabla\times\int_C\vec{M}(\vec{\rho}\,')\,H_0^{(2)}(k_{i+1}|\vec{\rho}-\vec{\rho}\,'|)\,dC'\right\}
\end{aligned}\tag{A1}$$

$$\begin{aligned}
&\hat{n}\times\left\{\vec{H}_i^{(exc)}(\vec{\rho})-\frac{\omega\epsilon_i}{4}\int_C\vec{M}(\vec{\rho}\,')H_0^{(2)}(k_i|\vec{\rho}-\vec{\rho}\,'|)\,dC'\right.\\
&\quad-\frac{1}{4\omega\mu_i}\cdot\nabla\int_C\nabla'\cdot\vec{M}(\vec{\rho}\,')H_0^{(2)}(k_i|\vec{\rho}-\vec{\rho}\,'|)\,dC'\\
&\quad\left.+\frac{1}{4j}\nabla\times\int_C\vec{J}(\vec{\rho}\,')H_0^{(2)}(k_i|\vec{\rho}-\vec{\rho}\,'|)\,dC'\right\}=\\
&\hat{n}\times\left\{\vec{H}_{i+1}^{(exc)}(\vec{\rho})+\frac{\omega\epsilon_{i+1}}{4}\int_C\vec{M}(\vec{\rho}\,')\,H_0^{(2)}(k_{i+1}|\vec{\rho}-\vec{\rho}\,'|)\,dC'\right.\\
&\quad+\frac{1}{4\omega\mu_{i+1}}\cdot\nabla\int_C\nabla'\cdot\vec{M}(\vec{\rho}\,')\,H_0^{(2)}(k_{i+1}|\vec{\rho}-\vec{\rho}\,'|)\,dC'\\
&\quad\left.-\frac{1}{4j}\nabla\times\int_C\vec{J}(\vec{\rho}\,')\,H_0^{(2)}(k_{i+1}|\vec{\rho}-\vec{\rho}\,'|)\,dC'\right\}
\end{aligned}\tag{A2}$$

where $\vec{\rho}'$ and $\vec{\rho}$ stand for the source and the observation points, whereas $\vec{J}(\vec{\rho}')$ and $\vec{M}(\vec{\rho}')$ are respectively the electric and magnetic equivalent surface current densities

on a dielectric interface $C$ between media, with constitutive parameters ($\epsilon_i$, $\mu_i$) and ($\epsilon_{i+1}$, $\mu_{i+1}$). On the other hand, ($\vec{E}_i^{(exc)}(\vec{\rho})$, $\vec{H}_i^{(exc)}(\vec{\rho})$) and ($\vec{E}_{i+1}^{(exc)}(\vec{\rho})$, $\vec{H}_{i+1}^{(exc)}(\vec{\rho})$) are the excitation fields on each side of the dielectric interface delimited by contour $C$, and are produced by point complex sources and/or equivalent surface currents corresponding to other material interfaces.

[43] On the other hand, the inner conducting reflectors are characterized by means of a Combined Field Integral Equation (CFIE) in order to avoid the internal resonance problem associated to either an Electric Field Integral Equation (EFIE) or a Magnetic Field Integral Equation (MFIE) [see *Peterson et al.*, 1998]. The CFIE is a linear combination of an EFIE and an MFIE, where a parameter $\alpha$ is used to adjust the weight of each integral equation. Nevertheless, for the particular case of an open reflector, $\alpha$ is set to one, since an MFIE can not inherently be formulated for the electromagnetic analysis of closed conductors. The general expression for the CFIE used to analyze the inner reflector inside the radome is given below:

$$\hat{n} \times \left\{ \alpha \vec{E}_i^{(exc)}(\vec{\rho}) + (1-\alpha)\vec{H}_i^{(exc)}(\vec{\rho}) \right\} = \hat{n} \times \left\{ \alpha \left[ \frac{\omega\mu_i}{4} \int \vec{J}(\vec{\rho}\,') H_0^{(2)}(k_i|\vec{\rho} - \vec{\rho}\,'|)\, dC' + \frac{1}{4\omega\epsilon_i} \nabla \int \nabla' \cdot \vec{J}(\vec{\rho}\,') H_0^{(2)}(k_i|\vec{\rho} - \vec{\rho}\,'|)\, dC' \right] + (1-\alpha) \cdot \left[ \vec{J}(\vec{\rho}\,') \times \hat{n} + \frac{1}{4j} \nabla \times \int \vec{J}(\vec{\rho}\,') H_0^{(2)}(k_i|\vec{\rho} - \vec{\rho}\,'|)\, dC' \right] \right\} \tag{A3}$$

where $\vec{J}(\vec{\rho}')$ is the induced surface electric current density on the reflector contour $C$, placed inside an homogenous medium with constitutive parameters ($\epsilon_i$, $\mu_i$). Moreover, ($\vec{E}_i^{(exc)}(\vec{\rho})$, $\vec{H}_i^{(exc)}(\vec{\rho})$) are the electromagnetic fields imposed on the conducting body by complex sources and/or equivalent currents on an adjacent interface between media. This last step completes the integral equation formulation used for the analysis of the radome problems presented in the paper.

[44] **Acknowledgments.** This work has been supported by Ministerio de Educacin y Ciencia, Spanish Government, under the Research Projects Ref. TEC2004/04313-C02-01 and TEC2004/04313-C02-02.

## References

Alpert, B., G. Beylkin, R. Coifman, and V. Rokhlin (1993), Wavelet-like bases for the fast solution of second-kind integral equations, *SIAM J. Sci. Comput.*, *44*(1), 159–184.

Arvas, E., and S. Ponnapalli (1989), Scattering cross section of a small radome of arbitrary shape, *IEEE Trans. Antennas Propag.*, *37*(5), 655–658.

Baharav, Z., and Y. Leviatan (1998), Impedance matrix compression (IMC) using iteratively selected wavelet basis, *IEEE Trans. Antennas Propag.*, *46*(2), 226–233.

Balanis, C. A. (1989), *Advanced Engineering Electromagnetics*, John Wiley, Toronto.

Chang, J.-H., and K.-K. Chan (1990), Analysis of a two-dimensional radome of arbitrarily curved surface, *IEEE Trans. Antennas Propag.*, *38*(10), 1565–1568.

Chen, K.-M. (1989), A mathematical formulation of the equivalence principle, *IEEE Trans. Microwave Theory Tech.*, *37*(10).

Davis, C. P., and K. F. Warnick (2005), Error analysis of 2-d mom for mfie/efie/cfie based on the circular cylinder, *IEEE Trans. Antennas Propag.*, *53*(1), 321–331.

Duan, D.-W., Y. Rahmat-Samii, and J. P. Mahon (1991), Scattering from a circular disk: a comparative study of PTD and GTD techniques, *Proc. IEEE*, *79*(10), 1472–1480.

Gao, X. J., and L. B. Felsen (1985), Complex ray analysis of beam transmission through two-dimensional radomes, *IEEE Trans. Antennas Propag.*, *33*(9), 963–975.

Hower, G. L., R. G. Olsen, J. D. Earls, and J. B. Schneider (1993), Inaccuracies in numerical calculation of scattering near natural frequencies of penetrable objects, *IEEE Trans. Antennas Propag.*, *41*(7), 982–986.

Hsu, C., and H. A. Auda (1986), Multiple dielectric posts in a rectangular waveguide, *IEEE Trans. Microwave Theory Tech.*, *34*(8), 883–891.

Kishk, A. A., and L. Shafai (1986), Different formulations for numerical solution of single or multibodies of revolution with mixed boundary conditions, *IEEE Trans. Antennas Propag.*, *34*(5), 666–673.

Kukobko, S. V., A. Z. Sazonov, and I. O. Sukharevsky (2005), Electrodynamic calculation method for two-dimensional model of a double-reflector antenna system with a nose dielectric radome, *Radio Phys. Radio Astron.*, *10*(2), 157–165.

Li, J.-Y., and L.-W. Li (2004), Characterizing scattering by 3-D arbitrarily shaped homogeneous dielectric objects using fast multipole method, *IEEE Antennas Wireless Propag. Lett.*, *3*, 1–4.

Lu, C.-C. (2003), A fast algorithm based on volume integral equation for analysis of arbitrarily shaped dielectric radomes, *IEEE Trans. Antennas Propag.*, *51*(3), 606–612.

Mautz, J., and R. F. Harrington (1979), Electromagnetic scattering from a homogeneous body of revolution, *A.E.U.*, *33*, 71–80.

Müller, C. (1969), *Foundations of the Mathematical Theory of Electromagnetic Waves*, Springer, Berlin.

Nosich, A. I. (1999), The method of analytical regularization in wave-scattering and eigenvalue problems: Foundations and review of solutions, *IEEE Antennas Propag. Mag.*, *41*(3), 982–986.

Oguzer, T. (2001), Analysis of circular reflector antenna covered by concentric dielectric radome, *IEEE Trans. Antennas Propag.*, *49*(3), 458–463.

Oguzer, T., A. Altintas, and A. Nosich (1995), Accurate simulation of reflector antennas by the complex source-dual series approach, *IEEE Trans. Antennas Propag.*, *43*(8), 793–801.

Oguzer, T., A. Nosich, and A. Altintas (2004), Analysis of an arbritrary conic section profile cylindrical reflector antenna, H-polarization case, *IEEE Trans. Antennas Propag.*, *52*(11), 3156–3162.

Peterson, A. F., S. L. Ray, and R. Mittra (1998), *Computational Methods for Electromagnetics*, IEEE Press, New York.

Poggio, A. J., and E. K. Miller (1973), *Integral Equation Solutions of Three-Dimensional Scattering Problems*, Pergamon, Oxford.

Sadigh, A., and E. Arvas (1992), Deformation of the horizontal radiation pattern of TV transmitting antennas due to thin dielectric radome, *IEEE Trans. Antennas Propag.*, *40*(8), 942–949.

Sarkar, T. K., and K. Kim (1999), Solution of large dense complex matrix equations utilizing wavelet-like transforms, *IEEE Trans. Antennas Propag.*, *47*(10), 1628–1632.

Sarkar, T. K., M. Salazar-Palma, and M. C. Wicks (2002), *Wavelet Applications in Engineering Electromagnetics*, Artech House, Norwood, Mass.

Steinberg, B. Z., and Y. Leviatan (1993), On the use of wavelet expansions in the method of moments, *IEEE Trans. Antennas Propag.*, *41*(5), 610–619.

Suedan, G. A., and E. V. Jull (1991), Beam difreaction by planar and parabolic reflectors, *IEEE Trans. Antennas Propag.*, *39*(4), 521–527.

Sukharevsky, O. I., S. V. Kukobko, and A. Z. Sazonov (2005), Volume integral equation analysis of a two-dimensional radome with a sharp nose, *IEEE Trans. Antennas Propag.*, *53*(4), 1500–1506.

Svezhentsev, A. Y., A. I. Nosich, and T. Oguzer (1995), Simulation of reflector antenna covered by a circular radome, in *Proceedings of ICAP'95 Ninth International Conference on Antennas and Propagation*, pp. 532–535, IEEE, New York.

Vidal, A., A. Belenguer, H. Esteban, V. E. Boria, C. Bachiller, and M. Taroncher (2004), Efficient and accurate spectral analysis of large scattering problems using wavelet and wavelet-like bases, *Radio Sci.*, *39*, RS5005, doi:10.1029/2003RS002991.

Wagner, R. L., and W. C. Chew (1995), A study of wavelets for the solution of electromagnetic integral equations, *IEEE Trans. Antennas Propag.*, *43*(8), 802–810.

Wang, G. (1995), A hybrid wavelet expansion and boundary element analysis of electromagnetic scattering from conducting objects, *IEEE Trans. Antennas Propag.*, *43*(2), 170–178.

Yurchenko, V., A. Altintas, and A. Nosich (1999), Numerical optimization of a cylindrical reflector-in-radome antenna system, *IEEE Trans. Antennas Propag.*, *47*(4), 668–673.

Zhao, W.-J., L.-W. Li, and Y.-B. Gan (2005), Efficient analysis of antenna radiation in the presence of airborne dielectric radomes of arbitrary shape, *IEEE Trans. Antennas Propag*, *53*(1), 442–449.

A. Alvarez-Melcón and F. D. Quesada-Pereira, Departamento de Tecnologías de la Información y las Comunicaciones, Technical University of Cartagena, E-30202 Cartagena, Spain.

V. E. Boria and A. Vidal, Departamento de Comunicaciones, Universidad Politécnica de Valencia, Camino de Vera s/n, E-46022 Valencia, Spain. (avidal@dcom.upv.es)

B. Gimeno, Departamento de Física Aplicada y Electromagnetismo-I.C.M.U.V., Universidad de Valencia, E-46100 Valencia, Spain.